Open access • Journal Article • DOI:10.1103/PHYSREVB.89.214510

Switching times in long-overlap Josephson junctions subject to thermal fluctuations and non-Gaussian noise sources — Source link

Davide Valenti, Claudio Guarcello, Bernardo Spagnolo

Institutions: University of Palermo

Published on: 23 Jun 2014 - Physical Review B (American Physical Society)

Topics: Josephson effect, Pi Josephson junction, Gaussian noise, Thermal fluctuations and Noise (signal processing)

Switching times in long-overlap Josephson junctions subject to thermal fluctuations and non-Gaussian noise sources

Davide Valenti,* Claudio Guarcello,† and Bernardo Spagnolo‡
Dipartimento di Fisica e Chimica, Group of Interdisciplinary Physics, Università di Palermo and CNISM, Unità di Palermo Viale delle Scienze, Edificio 18, I-90128 Palermo, Italy
(Received 19 March 2014; revised manuscript received 2 June 2014; published 23 June 2014)

We investigate the superconducting lifetime of long current-biased Josephson junctions, in the presence of Gaussian and non-Gaussian noise sources. In particular, we analyze the dynamics of a Josephson junction as a function of the noise signal intensity, for different values of the parameters of the system and external driving currents. We find that the mean lifetime of the superconductive state is characterized by nonmonotonic behavior as a function of noise intensity, driving frequency, and junction length. We observe that these nonmonotonic behaviors are connected with the dynamics of the junction phase string during the switching towards the resistive state. An important role is played by the formation and propagation of solitons, with two different dynamical regimes characterizing the dynamics of the phase string. Our analysis allows to evidence the effects of different bias current densities, that is a simple spatially homogeneous distribution and a more realistic inhomogeneous distribution with high current values at the edges. Stochastic resonant activation, noise-enhanced stability, and temporary trapping phenomena are observed in the system investigated.

DOI: 10.1103/PhysRevB.89.214510 PACS number(s): 85.25.Cp, 05.10.Gg, 72.70.+m, 74.40.−n

I. INTRODUCTION

During past decades the interest in superconductor physics and its applications has had a remarkable development. In this context an important role is played by improvements made in devising and realizing Josephson junction (JJ)-based devices. In fact, great attention has been paid to JJs as superconducting quantum bits [1–4], nanoscale superconducting quantum interference devices for detecting weak flux changes [5,6], and threshold noise detectors [7–10]. Moreover, JJs are typical out-of-equilibrium systems characterized by tilted or switching periodic potentials [11,12].

The behavior of these systems is strongly influenced by environmental perturbations and specifically by the presence of a noise source responsible for decoherence phenomena [2,13]. The role played by random fluctuations in the dynamics of these devices has recently solicited a large amount of work and investigation on the effects both of thermal and nonthermal noise sources on the transient dynamics of Josephson junctions [14–19]. The noise current signal is caused by the stochastic motion of the charge carriers, namely the Cooper pairs in a superconductor. While thermal noise is originated by the thermal motion of the charge carriers, nonthermal noise signals are related to their scattering and transmission. Non-Gaussian noise appears when the conductor, or the superconductor, is in a nonequilibrium state because of the presence of a bias voltage or current. In the past decade, theoretical progress allowed one to calculate the entire probability distribution of the noise signal and its cumulants, and to perform a *full counting statistics* of the current fluctuations [15]. Moreover, the presence of non-Gaussian noise signals has been found experimentally in many systems [14,18,20–23]. As an example in a wireless ad hoc network with a Poisson field of co-channel users, the noise has been well modeled by an α-stable distribution [23]. A nonequilibrated heat reservoir can be considered a source of non-Gaussian noises [20–22]. Specifically, the effect of non-Gaussian noise on the average escape time from the superconducting metastable state of a current-biased JJ, coupled with nonequilibrium current fluctuations, was experimentally investigated [14,18].

Recently, the characterization of JJs as detectors, based on the statistics of the escape times, was proposed [7–10,24–26]. Specifically, the statistical analysis of the switching from the metastable superconducting state to the resistive running state of the JJ has been proposed to detect weak periodic signals embedded in a noise environment [9,10]. Moreover, the rate of escape from one of the metastable wells of the tilted washboard potential of a JJ encodes information about the non-Gaussian noise present in the input signal [7,8,24–26].

Motivated by these studies and the importance of the problem of the transient dynamics of a JJ interacting with a noisy environment, we try to understand how non-Gaussian noise sources affect the switching times in long JJs. In light of this, our work is devoted to investigate the response of a superconductive device to the solicitations of both deterministic and stochastic external perturbations, due to thermal fluctuations [27–29] or connected with the variability of bias current and magnetic field [14,18]. In particular, we analyze the system dynamics, modeling environmental random fluctuations by noise sources with different, Gaussian and non-Gaussian, statistical distributions. The superconducting device is a long Josephson junction (LJJ), which is a device in which one dimension is much longer than the Josephson penetration depth λ_J of the junction. The JJs considered in our study are arranged in the *overlap* geometrical configuration. These devices can work in two different conditions: (i) the superconducting regime, which corresponds to the localization of the order parameter, that is, the phase difference across the junction, in a metastable state of the washboard potential, and (ii) the resistive regime with a dissipative voltage-current relation,

*davide.valenti@unipa.it
†claudio.guarcello@unipa.it
‡bernardo.spagnolo@unipa.it

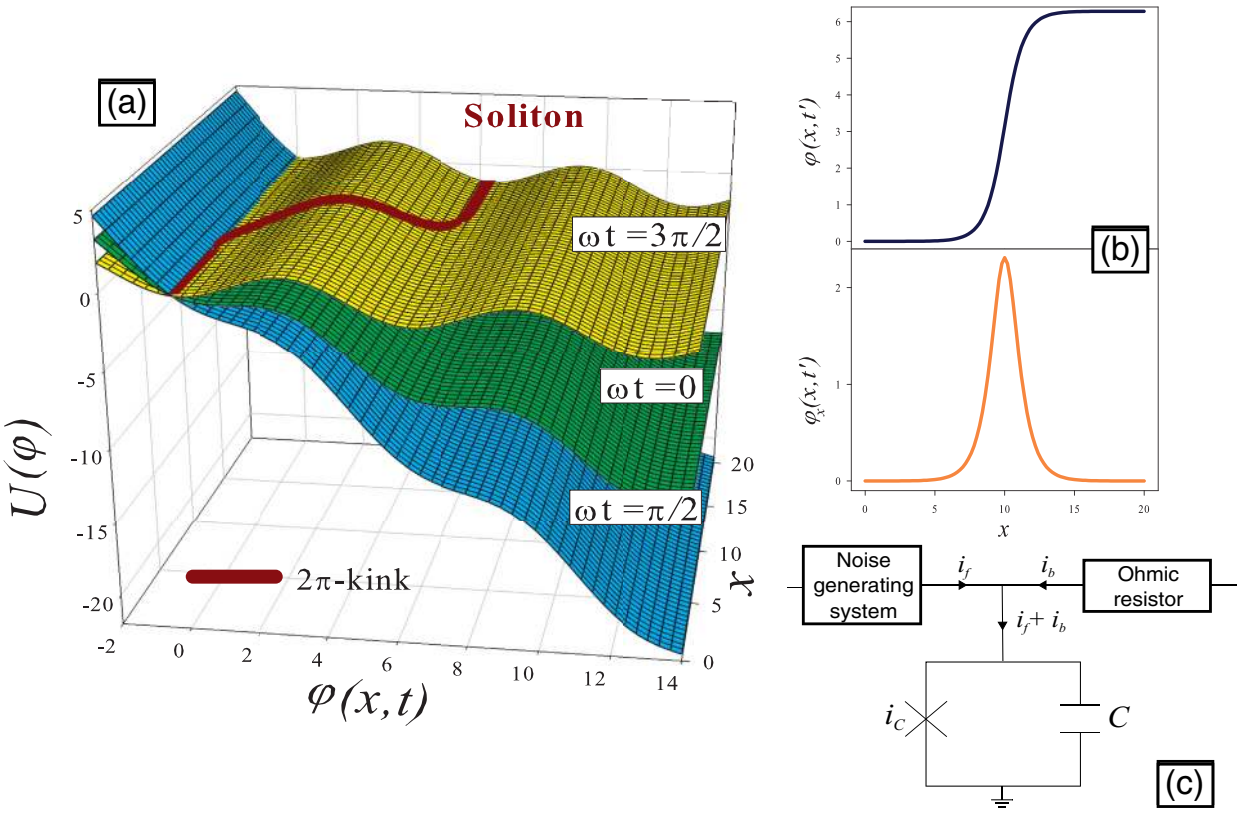

FIG. 1. (Color online) (a) Washboard potential at three different times with a soliton wave (2π kink) on the highest profile, (b) soliton [Eq. (9)] and corresponding fluxon profile [Eq. (10)], and (c) circuit diagram of a JJ noise detector: a JJ with critical current i_C is biased in a twofold way.

corresponding to an escape event of the phase difference from the metastable state [see Fig. 1(a)]. The superconductive phase is subject to both thermal and non-Gaussian noise, due to an external driving force. We note that the effects of Gaussian [27–31] and non-Gaussian [7,8,24,25,32] noise sources on short JJs have been thoroughly studied, whereas analyses of the phase dynamics of long JJs have been performed only in the presence of thermal fluctuations [33–36]. Moreover, noise-induced effects due to thermal fluctuations, such as *resonant activation* (RA), or *stochastic resonant activation* [37,38], and *noise-enhanced stability* [39,40] (NES), have been theoretically predicted in overdamped JJs [27–32] and experimentally in underdamped JJs [41–43]. It is worthwhile to note that experimental works on the realization of overdamped JJ with nonhysteretic current voltage and high temperature stability have been performed [44].

After the seminal paper of Tobiska and Nazarov [19], Josephson junctions used as threshold detectors allow the study of non-Gaussian features of current noise [24,25]. Specifically, when a JJ leaves the metastable zero-voltage state it switches to a running resistive state and a voltage appears across the junction. Therefore, it is possible to measure directly in experiments the escape times or switching times and to determine their probability distribution [41–43,45–47]. A typical simplified realization of a JJ noise detector is shown in Fig. 1(c). The fluctuating current i_f, produced by the noise-generating system, is added to the bias current i_b and drives the JJ, characterized by a critical current i_C and a capacitance C. The switching times of the junction can be directly measured using the time-domain technique [41–43,48,49]. For each switching event the bias current is ramped up to a value i_b, which is very close to the critical current i_C and it is maintained constant for a period of waiting time. To record the switching time, the voltage across the junction is sent to a timer counter, which is triggered by the sudden jump from zero-voltage state to finite-voltage state. The bias current is then decreased to zero, the junction returns to the zero-voltage state, and a new cycle starts again. For JJs working in an overdamped regime, the superconducting state is restored automatically, without the necessity to decrease the bias current to zero. The process is repeated enough times to obtain a statistically significant ensemble of switching times (STs). The typical frequency range of a detector of non-Gaussian noise, based on a long JJ working in an overdamped regime, as in our investigation, is from 10 to 600 GHz. Of course, higher frequencies can be obtained with a long JJ in overlap geometry, but the experimental setup should be more complicated and would be very expensive. Concerning the physical range of feasibility of the other main parameters of the junction, typical values are JJ length L from $0.1\lambda_J$ to $20\lambda_J$, with the Josephson penetration depth λ_J in the range [10, 20] μm, and range of the critical current [5, 15] mA.

In this paper we investigate how the simultaneous action of an external oscillating driving force and a fluctuating signal affects the permanence time inside the metastable state of a LJJ. In particular, we concentrate on the escape time, that is,

the time the junction takes to switch from the superconducting state to the resistive regime, calculating the *mean switching time* (MST) obtained by averaging over a sufficiently large number of numerical realizations. The analysis is performed varying also the frequency of the driving current, the length of the junction, and the amplitude of the noise signal modeled by using different α-stable (or *Lévy*) distributions. These statistics allow to describe real situations [50] in which the evolution shows abrupt jumps and very rapid variations of parameters, called *Lévy flights*. Lévy-type statistics is observed in various scientific areas, where scale-invariance phenomena take place [51–54]. For a recent short review on Lévy flights see the work by Dubkov *et al.* [55] and references therein. Applications and other research fields in which observed evolutions are well reproduced using Lévy statistics are quite numerous, ranging from biology [56], zoology [57–59], social systems [60], and financial markets [61] to geological [62] and atmospheric data [63].

The dynamics of the phase difference of the LJJ, analyzed within the sine-Gordon (SG) formalism [34,35,64,65], is characterized by the formation and propagation of particular wave packets called *solitons* [66,67]. Their presence is strongly connected with the penetration of the magnetic flux quanta, i.e., *fluxons* [68,69] (the magnetic soliton), traveling through the junction during the switching towards the resistive state [see Fig. 1(b)]. Here we recall that several systems governed by the SG equation show evidence of soliton motion, including not only JJs [70–76] but also the relativistic field theory, mechanical transmission lines, and atomic, particle, and condensed matter physics. A peculiar dynamics is also present in the superconducting device analyzed in this work.

Finally, it is worth nothing that for low phase values, $\sin(\varphi) \approx \varphi$, the SG equation approaches the Klein-Gordon one [77]. Nevertheless, the exact solutions are known only for the simplest *unperturbed* SG differential equation, in the absence of damping, driving, and fluctuating terms [64].

The paper is organized as follows. In the next section the sine-Gordon model is presented. In Sec. III we briefly review the statistical properties of the Lévy noise, showing some peculiarities of different α-stable distributions. Section IV gives computational details. In Sec. V the theoretical results for the behaviors of the MST as a function of the junction length, frequency of the external driving current, and noise intensity with homogeneous and inhomogeneous bias current are shown and analyzed. This analysis was carried out at very low temperatures of the system, around the *crossover* temperature.

Below this temperature, the phase difference over the junction behaves quantum mechanically, the escape events occur primarily by quantum tunneling through the barrier, and the thermal fluctuations can be neglected. Therefore, only the effects of non-Gaussian noise were analyzed. The transient dynamics of a long JJ subject to thermal fluctuations and non-Gaussian, Lévy-type, noise sources is investigated in Sec. VI. Finally, in Sec. VII we draw conclusions.

II. THE SG MODEL

The electrodynamics of a normal JJ is described by a nonlinear partial differential equation for the order parameter φ, that is, the sine-Gordon equation [64,65]. Here φ is the phase difference between the wave functions describing the superconducting condensate in the two electrodes. Our analysis includes a quasiparticle tunneling term and an additional stochastic contribution, $i_f(x,t)$, representing the noise effects. However, the surface resistance of the superconductors is neglected. The resulting *perturbed* SG equation reads

$$\begin{aligned}\beta_{\mathrm{SG}}\varphi_{tt}(x,t) + \varphi_t(x,t) - \varphi_{xx}(x,t) \\ = i_b(x,t) - \sin(\varphi(x,t)) + i_f(x,t),\end{aligned} \tag{1}$$

where a simplified notation has been used, with the subscript indicating the partial derivative of φ in that variable. This notation is used throughout the paper. In Eq. (1), the fluctuating current density $i_f(x,t)$ is the sum of two contributions, a Gaussian thermal noise $i_T(x,t)$ and an external non-Gaussian noise source $i_{nG}(x,t)$:

$$i_f(x,t) = i_T(x,t) + i_{nG}(x,t). \tag{2}$$

The SG equation is written in terms of the dimensionless x and t variables, which are the space and time coordinates normalized respectively to the Josephson penetration depth λ_J and to the inverse of the characteristic frequency ω_J of the junction. Moreover, $\beta_{\mathrm{SG}} = \omega_J RC$, where R and C are the effective normal resistance and capacitance of the junction. The terms $i_b(x,t)$ and $\sin(\varphi)$ of Eq. (1) are respectively the bias current and supercurrent, both normalized to the JJ critical current i_C. Equation (1) is solved by imposing the following boundary conditions:

$$\varphi_x(0,t) = \varphi_x(L,t) = \Gamma, \tag{3}$$

where Γ is the normalized external magnetic field. Hereinafter we impose $\Gamma = 0$.

The two-dimensional time-dependent tilted potential, called the *washboard potential*, is given by

$$U(\varphi,x,t) = 1 - \cos(\varphi(x,t)) - i_b(x,t)\,\varphi(x,t), \tag{4}$$

and shown in Fig. 1(a). In the same figure is shown a phase string in the potential profile (4), along which it moves during the switching dynamics. Specifically, the washboard potential is composed of a periodical sequence of peaks and valleys, with minima and maxima satisfying the following conditions:

$$\begin{aligned}\varphi_{\min} &= \arcsin(i(x,t)) + 2n\pi, \\ \varphi_{\max} &= (\pi - \arcsin(i(x,t))) + 2n\pi,\end{aligned} \tag{5}$$

with $n = 0, \pm 1, \pm 2, \ldots$.

The bias current is given by

$$i_b(x,t) = i_b(x) + A\ \sin(\omega t), \tag{6}$$

where A and ω are amplitude and frequency (normalized to ω_J) of the dimensionless driving current. This time dependence is normalized to the inverse of the JJ characteristic frequency ω_J.

The $i_b(x)$ term is a dimensionless current that, in the phase string picture, represents the initial slope of the potential profile. Different regimes of spatial dependence can be considered, obtaining in particular the two following current distributions [78]:

$$i_b(x) = \begin{cases} i_0, & \text{homogeneous} \\ \frac{i_0\,L}{\pi\sqrt{x\,(L-x)}}, & \text{inhomogeneous.} \end{cases} \tag{7}$$

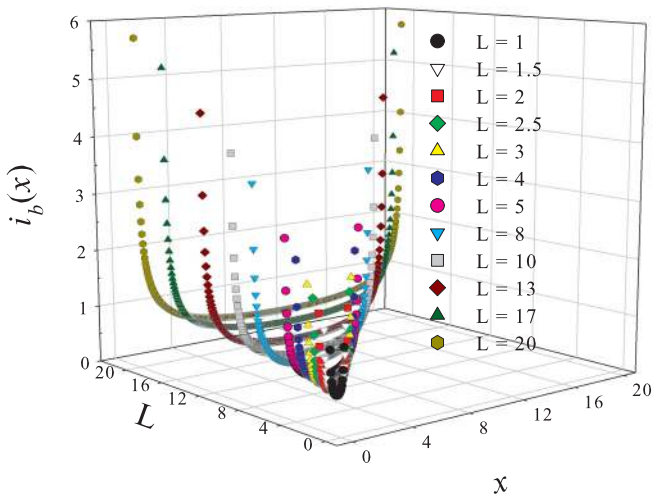

FIG. 2. (Color online) Inhomogeneous bias current density [see Eq. (7)] along JJs, for $i_0 = 0.9$ and different values of junction length.

The more realistic inhomogeneous condition provides strong current contributions at the edges of the junction. This is shown in Fig. 2, for $i_0 = 0.9$ and L ranging between 1 and 20. In these conditions, the phase of the cells in the edges of the junction can flow along the potential without resistance, so that the soliton formation occurs mostly in these parts of the junction.

The unperturbed SG equation, in the absence of damping, bias, and noise, is given by

$$\varphi_{xx}(x,t) - \varphi_{tt}(x,t) = \sin(\varphi(x,t)). \tag{8}$$

This equation admits solutions in the traveling wave form $f = \varphi(x - ut)$ [64]:

$$\varphi(x - ut) = 4\arctan\left\{\exp\left[\pm\frac{(x-ut)}{\sqrt{1-u^2}}\right]\right\}, \tag{9}$$

where u is the wave propagation velocity normalized to the speed of light and is called the *Swihart velocity*. Equation (9) represents a single *kink*, or *soliton*, that is a 2π variation in the phase values. The signs $+$ and $-$ indicate the two opposite directions of propagation, corresponding to 2π kink (soliton) and 2π antikink (antisoliton), respectively. In this framework, φ gives a normalized measure of the magnetic flux through the junction, so that Eq. (8) can also represent the motion of a single fluxon (or antifluxon). In fact, starting from simple electrodynamic considerations [64], it is possible to obtain a simple relation between the magnetic field $H(y)$ and the spatial derivative of the phase difference,

$$\varphi_x = \frac{2e}{\hbar c} dH(y), \tag{10}$$

where $d = \lambda_L + \lambda_R + t$ is the magnetic penetration, λ_L and λ_R are the London depths in the left and right superconductors, and t is the interlayer thickness. In our LJJ model, if the junction is extended along x and short along z, the magnetic field points along y, so that $H(y) \equiv H$. Integrating Eq. (10) over the entire JJ length, the following relation is obtained:

$$\varphi(L) - \varphi(0) = \frac{2e}{\hbar c}\Phi_H = 2\pi\frac{\Phi_H}{\Phi_0}, \tag{11}$$

where Φ_H is the magnetic flux through the junction and $\Phi_0 = hc/2e$ is the fluxon. If the phase string has a portion lying in the first valley and a portion inside the nth valley, from Eq. (5), the phase difference is equal to $2\pi n$. Therefore, the magnetic flux will be equal to

$$2\pi n = 2\pi\frac{\Phi_H}{\Phi_0}, \quad \Phi_H = n\Phi_0. \tag{12}$$

If the phase evolution shows a single 2π kink, a single fluxon will propagate along the junction, as shown in Fig. 1(b). Here the washboard potential is represented at three different times $t = 0, \frac{\pi}{2\omega}, \frac{3\pi}{2\omega}$, corresponding to zero initial slope, and maximum and minimum slope, respectively. The line on the highest potential profile represents a soliton between two adjacent valleys. Figure 1(b) shows a soliton and the shape of the correspondent fluxon, that is, the values of the x derivative of φ, along the junction length in a generic time t'.

III. THE LÉVY STATISTICS

In order to motivate the use of α-stable (or Lévy) distributions we recall some cases [79] in which non-Gaussian stable statistics is used to model experimental data with asymmetric and heavy-tailed distributions, closely linked with the generalized central limit theorem [80–86]. Here we briefly review the concept of stable distribution. A random nondegenerate variable is stable if

$$\forall n \in \mathbb{N}, \quad \exists(a_n, b_n) \in \mathbb{R}^+ \times \mathbb{R} : \quad X + b_n = a_n \sum_{j=1}^{n} X_j, \tag{13}$$

where the X_j terms are independent copies of X. Moreover, X is strictly stable if and only if $b_n = 0, \ \forall n$. The well-known Gaussian distribution stays in this class. This definition does not provide a parametric handling form of the stable distributions. The characteristic function, however, allows for dealing with them. The general definition of a characteristic function for a random variable X with an associated distribution function $F(x)$ is

$$\phi(u) = \langle e^{iuX}\rangle = \int_{-\infty}^{+\infty} e^{iuX} dF(x). \tag{14}$$

Following this statement, a random variable X is said to be stable if and only if

$$\exists(\alpha,\sigma,\beta,\mu) \in]0,2] \times \mathbb{R}^+ \times [-1,1] \times \mathbb{R} : \quad X \overset{d}{=} \sigma Z + \mu, \tag{15}$$

where Z is a random number. Accordingly one obtains

$$\phi(u) = \begin{cases} \exp\left\{-|u|^\alpha\left[1 - i\beta\tan\frac{\pi\alpha}{2}(\mathrm{sign}u)\right]\right\}, & \alpha \neq 1 \\ \exp\left\{-|u|\left[1 + i\beta\frac{2}{\pi}(\mathrm{sign}u)\log|u|\right]\right\}, & \alpha = 1, \end{cases} \tag{16}$$

in which

$$\mathrm{sign}u = \begin{cases} \pm 1, & u \gtrless 0 \\ 0, & u = 0, \end{cases} \tag{17}$$

represents the sign function.

TABLE I. Closed form of the stable distributions and characteristic values of parameters.

Distribution	Abbreviation	$P(x)$		$S_\alpha(\sigma,\beta,\mu)$
Gaussian	(G)	$\frac{1}{\sqrt{2\pi}\sigma} e^{-\frac{(x-\mu)^2}{2\sigma^2}}$	$x \in \mathbb{R}$	$S_2(\sigma,0,\mu)$
Cauchy-Lorentz	(CL)	$\frac{\sigma/\pi}{\sigma^2+(x-\mu)^2}$	$x \in \mathbb{R}$	$S_1(\sigma,0,\mu)$
Lévy-Smirnov	(LS)	$\sqrt{\frac{\sigma}{2\pi}} \frac{e^{-\frac{\sigma}{2(x-\mu)}}}{(x-\mu)^{3/2}}$	$x \geqslant \mu$	$S_{\frac{1}{2}}(\sigma,1,\mu)$

This definition of X requires four parameters: a *stability index* (or characteristic exponent) $\alpha \in]0,2]$, an *asymmetry parameter* β with $|\beta| \leqslant 1$, and two real numbers $\sigma > 0$ and μ that determine the outward shape of the distribution and are called, for this reason, *shape parameters*. The names of these two parameters indicate their physical meaning. Specifically $\beta = 0$ ($\beta \neq 0$) gives a symmetric (asymmetric) distribution, while α determines how the tails of the distribution go to zero. For $\alpha < 2$ the asymptotic behavior is characterized by a power law, while $\alpha = 2$ and $\beta = 0$ give a Gaussian distribution. The stable distribution, obtained by setting $\sigma = 1$ and $\mu = 0$, is called *standard*. We denote every α-stable distribution with the symbol $S_\alpha(\sigma,\beta,\mu)$. Only a few Lévy distributions have a probability density function known in explicit form, as shown in Table I. Here the abbreviations for some peculiar distributions, used in the rest of this work, are also listed. The G (Gaussian) and CL (Cauchy-Lorentz) distributions (both with $\beta = 0$) are symmetrical with respect to $x = 0$, while the LS (Lévy-Smirnov) distributions (normal and reflected) are skewed to the right ($\beta = +1$) or left ($\beta = -1$) side. The three distributions of Table I are plotted in Fig. 3. The reflected (with respect to the vertical axis) LS distribution, obtained by setting $\beta = -1$, is not shown. The asymmetrical structure of the LS distribution is evident, with a heavy tail and a narrow peak located at a positive value of x. The CL distribution, in comparison with the Gaussian one, presents tails much higher and a central part of the distribution more concentrated around the mean value. For short times, the values extracted from a CL distribution determine trajectories characterized by *limited space displacement*: this can be explained by noting that the CL statistics is characterized, around the mean, by a narrower form with respect to the Gaussian one. For longer times, however, heavy tails cause the occurrence of events with large values of x, whose probability densities are non-neglectable. The use of CL and LS statistics allows the consideration of rare events, corresponding to large values of x, because of the fat tails of these distributions. These events correspond to the Lévy flights previously discussed. The algorithm used in this work to simulate Lévy noise sources is that proposed by Weron [87] for the implementation of the Chambers method [88].

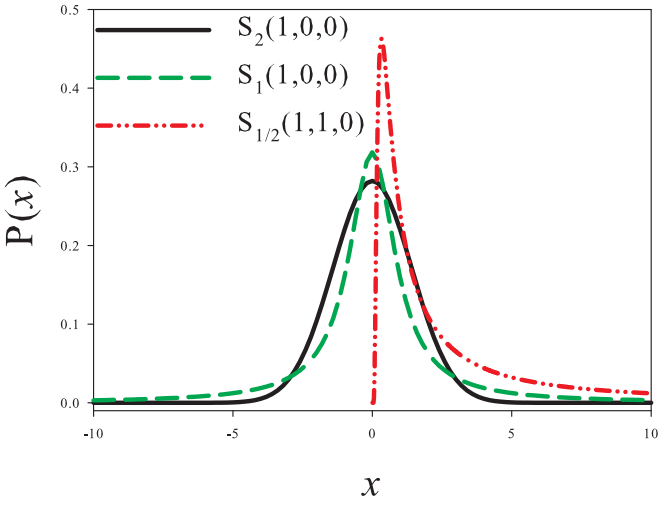

FIG. 3. (Color online) Probability density functions for Gaussian (solid line), Cauchy-Lorentz (dashed line), and Lévy-Smirnov (dash-dotted line) distributions.

IV. COMPUTATIONAL DETAILS

We study the JJ dynamics in the SG overdamped regime, setting $\beta_{SG} = 0.01$. The time and spatial steps are fixed at $\Delta t = 0.05$ and $\Delta x = 0.05$. In order to obtain the mean values we perform a suitable number ($N = 5000$) of numerical realizations. Throughout the whole paper we use the words *string*, referring to the entire junction, and *cell*, indicating each of the elements with dimension Δx, which compose the junction. The washboard potential valley labeled with $n = 0$ [Eq. (5)] is chosen as an initial condition for solving Eq. (1); i.e., $\varphi_0 = \arcsin(i_b(x,0)) = \arcsin(i_b(x))$. In our model there are no barriers, either absorbing or reflecting, surrounding the initial metastable state, and the value of MST calculated is the nonlinear relaxation time (NLRT) [89]. After a first exit, other temporary trapping events are permitted: during the time evolution each cell can return to the initial potential well, contributing again to the final value of MST, indicated as τ. This agrees with the definition, proposed by Malakhov [90], for the mean permanence time of the phase φ inside the interval $[-\pi,\pi]$:

$$\tau = \int_0^\infty t w(t) dt = \int_0^\infty P(t) dt, \tag{18}$$

where $P(t)$ is the probability that $\varphi \in [-\pi,\pi]$ and $w(t) = \partial P(t)/\partial t$. For each cell and for each realization the numerical calculation of $P(t)$ is performed by considering

$$P_{ij}(t) = \begin{cases} 1 \iff \varphi \in [-\pi,\pi] \\ 0 \iff \varphi \notin [-\pi,\pi], \end{cases} \tag{19}$$

where P_{ij} is the probability that in the ith realization for the jth cell $\varphi \in [-\pi,\pi]$. Summing $P_{ij}(t)$ over the total number N_{cells} of string elements, and averaging first over the total number of cells, then over the total number N of realizations, we find the probability that the entire string is in the superconducting state at time t:

$$P(t) = \frac{1}{N\, N_{\text{cells}}} \sum_{i=1}^{N} \sum_{j=1}^{N_{\text{cells}}} P_{ij}(t) \tag{20}$$

The maximum time value used to perform the integral of Eq. (18) has to be set large enough so that temporary trapping events, in the metastable state, can occur. Therefore, we replace the upper limit of the integral, ∞, with a maximum time $t_{\max} = 100$, obtaining the *mean switching time*

$$\tau = \int_0^{t_{\max}} P(t) dt. \tag{21}$$

The whole procedure is repeated for the three noise statistics analyzed in the previous section, obtaining the behavior of the MST τ in the presence of different sources of Lévy noise.

V. EFFECTS OF NON-GAUSSIAN NOISE

The analysis is carried out looking at the MST variations as a function of the junction length L, noise intensity γ, and frequency ω of the driving signal. The i_0 values chosen are 0.5 and 0.9, so that we can work with potentials less or more inclined, and the $i_b(x)$ distributions used are homogeneous or inhomogeneous [Eq. (7)]. The washboard slope is connected to the heights of the potential barriers seen by the phase elements. Reducing the i_0 value, the barrier's intensity is enhanced and the MST values tend to increase. We search for evidence of nonmonotonic behavior by varying first the values of L, γ, and ω, then the statistics of the noise sources. Moreover, we try to find connections between the MST behaviors and JJ soliton dynamics. The amplitude of the oscillating driving signal is set to $A = 0.7$, to obtain at certain times [see Eq. (6)] $i_b(x,t) > 1$ (absence of metastable states) and, at least with one of the i_0 values used, $i_b(x,t) < 0$ (positive slope). In this section we neglect the thermal fluctuations of the current density $i_T(x,t)$ with respect to the non-Gaussian (Lévy) noise source $i_{nG}(x,t)$ in Eqs. (1) and (2), because we consider very low temperatures, around the *crossover* temperature.

A. MST versus JJ length L

We begin to study the MST values varying the JJ length L in the range $[0,20]$. The results are shown in Fig. 4, emphasizing the three different noise sources used: G [Figs. 4(a) and 4(d)], CL [Figs. 4(b) and 4(e)], and LS [Figs. 4(c) and 4(f)].

Figures 4(a)–4(c) contain the results for homogeneous bias current density, while Figs. 4(d)–4(f) contain the results for inhomogeneous bias current density. In each panel, we note that the MST values for $i_0 = 0.5$ are greater than those for $i_0 = 0.9$. This is due to the reduced height of the right potential barrier due to the increased slope, i.e., the i_0 value, of the washboard. Specifically the expression for the left (or right) potential barrier height ΔU^+(or ΔU^-) is

$$\Delta U^{\pm}(x,t) = 2\sqrt{1 - i_b^2(x,t)} + i_b(x,t)[2\arcsin(i_b(x,t)) \pm \pi]. \quad (22)$$

We start analyzing the results obtained in the presence of a Gaussian noise source with $i_0 = 0.5$ and $i_b(x)$ homogeneous [open symbols in Fig. 4(a)]. In this panel of Fig. 4 the presence of two different dynamical regimes in each of these curves is evident. An initial monotonic increasing behavior is followed by a constant MST plateau. This underlines the presence of two different mechanisms, governing the time evolution of the phase, which clearly appear in the soliton dynamics shown in Fig. 5. This figure displays four different phase dynamics during the passage towards the resistive state, i.e., when the phase φ approximately changes by 2π. The cells can escape from a potential well altogether [Fig. 5(a)] or by the formation of a single kink, or a single antikink, or a kink-antikink (K-A) pair [Fig. 5(c)]. If the string is too short, the connection among cells is so strong that the soliton formation is forbidden, and the string can move from, or remain inside, a potential minimum as a whole. This is evident in Fig. 5(a). In this length regime, an increase in the number of cells makes more difficult the motion

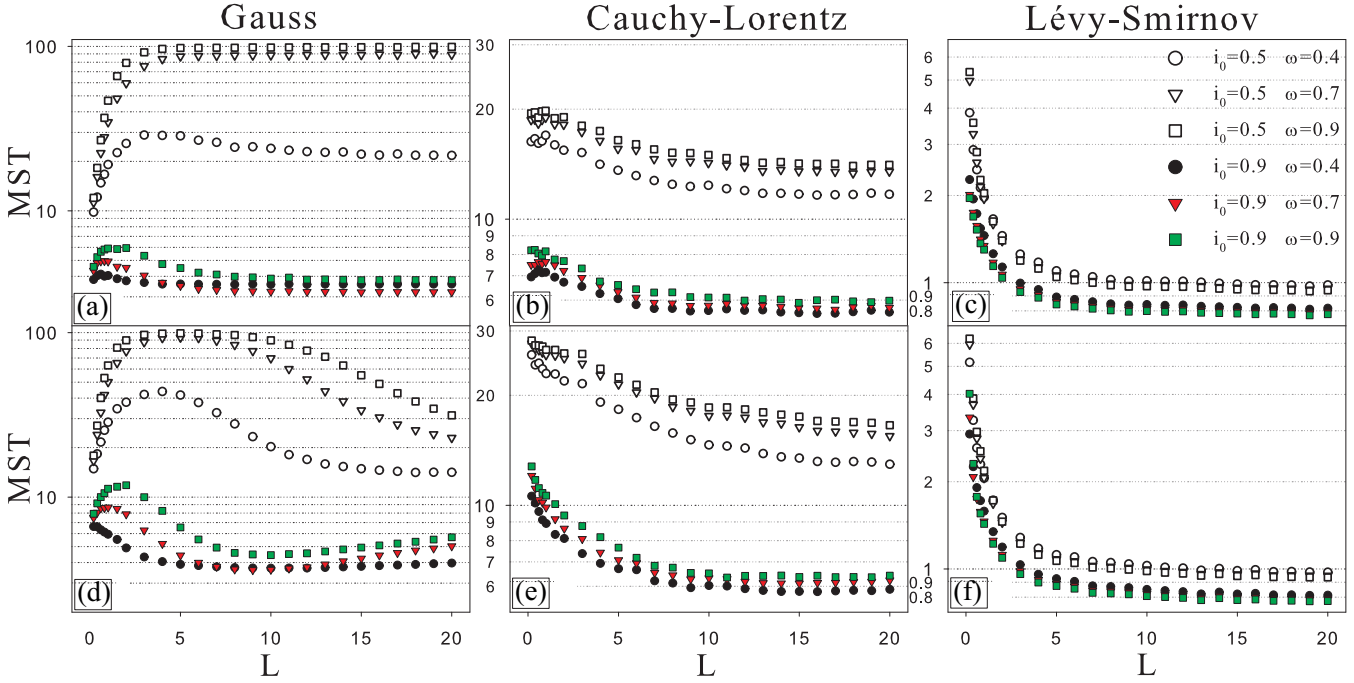

FIG. 4. (Color online) MST τ vs L for different current distributions along the junction: homogeneous $i_b(x)$ and noise sources with (a) Gaussian, (b) Cauchy-Lorentz, and (c) Lévy-Smirnov statistics; inhomogenous $i_b(x)$ and noise sources with (d) Gaussian, (e) Cauchy-Lorentz, and (f) Lévy-Smirnov statistics. In all graphs the other parameters are $i_0 = \{0.5$ (open symbols),0.9 (solid symbols)$\}$, $\omega = \{0.4$ (circles),0.7 (triangles),0.9 (squares)$\}$, and $\gamma = 0.2$. The legend in (c) refers to all figures.

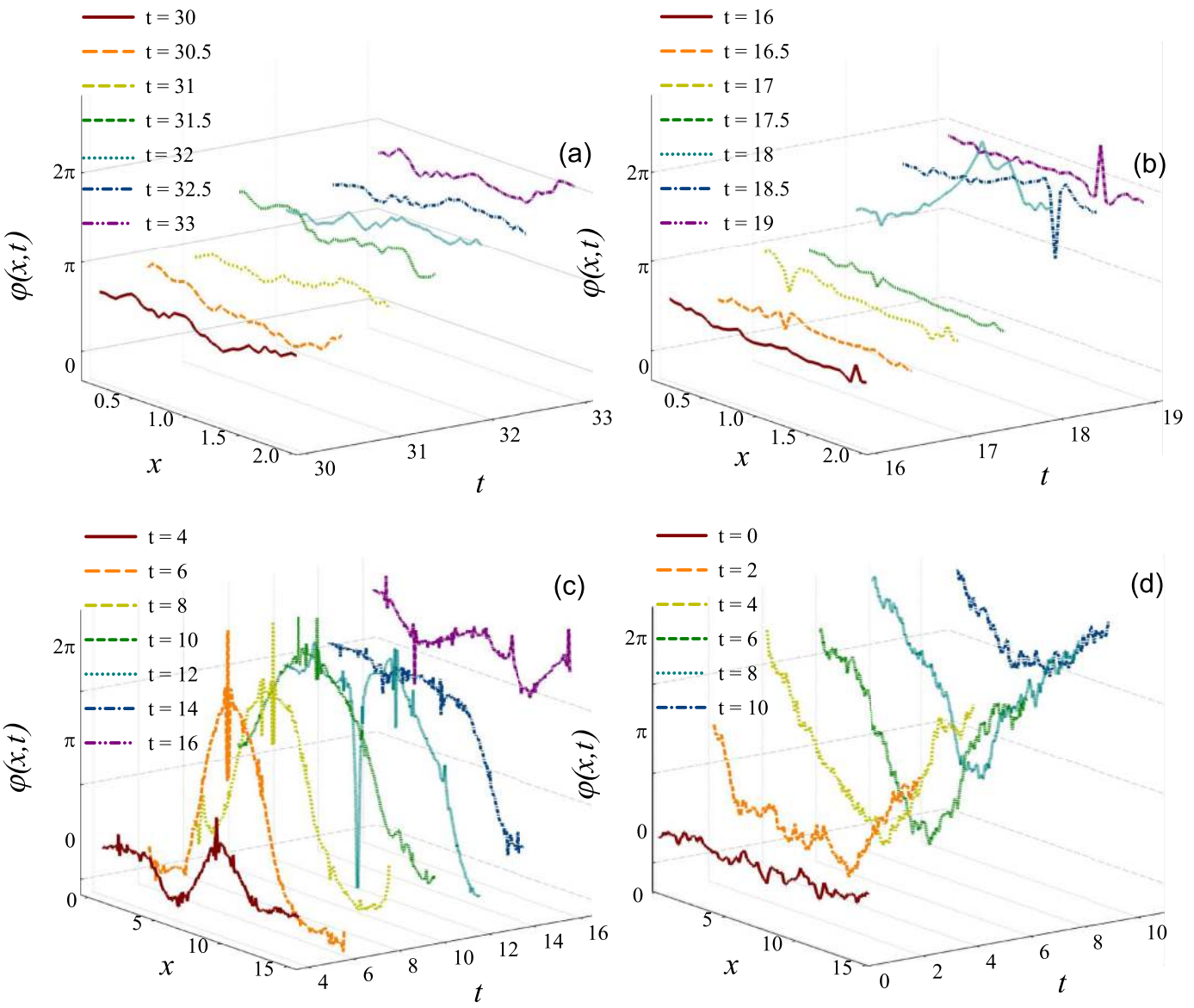

FIG. 5. (Color online) String dynamics during the switching towards the resistive state, for a JJ of length $L = 2$, with (a) homogeneous bias current distribution and G noise source, and (b) inhomogeneous bias current distribution and CL noise source, and for a JJ of length $L = 15$, with (c) homogeneous bias current distribution and CL noise source, and (d) inhomogeneous bias current distribution and G noise source. All graphs were obtained for $\omega = 0.9$ and $\gamma = 0.2$. The curves in panels (b) and (c) show the characteristic Lévy flights of the CL statistic.

of the whole string during the transition process, causing the MST to raise for short lengths. This happens as long as no soliton formation occurs. There is, in fact, a specific junction length above which the dynamics is governed by the formation of phase kinks. This length is connected with the soliton nucleation, that is, the formation of a K-A pair. Following the work of Büttiker [67], in the soliton nucleation a critical nucleus, which is the minimum separation between kink and antikink, exists. For junction lengths greater than this critical value, a saturation effect is evident. The MST reaches an almost constant value and the switching events are guided by the solitons, which indicates that the dynamics of these events is independent of the JJ length. To explain this behavior we consider that inside the string a subdomain structure exists. Each subdomain is composed by an amount of cells of total size approximately equal to the critical nucleus. The entire string can be thought of as the sum of these subdomains and the overall escape event results in the superimposition of the escape events of each single subdomain, so that the total MST is equal to the individual subdomain time evolution. The size of this subdomain approximately corresponds to the length value for which the initial monotonic behavior is interrupted. The dimension of the critical nucleus is proportional to $L_c \propto -\log(i_0)$. Increasing the i_0 value, the critical nucleus decreases and the soliton dynamics can start in correspondence of shorter junction lengths, as one can see in Fig. 4(a), where results obtained for $i_0 = 0.5$ (open symbols) and $i_0 = 0.9$ (solid symbols) are shown. In particular, we have $L_c \sim 5$ for $i_0 = 0.5$, and $L_c \sim 2$ for $i_0 = 0.9$. The curves obtained for $i_0 = 0.9$ are characterized by a small maximum, which reveals

the presence of a weak nonmonotonic behavior. Between the initial increasing behavior and the saturation, a portion with negative slope and corresponding reduction of the MST is evident. Increasing the slope of the potential, the critical nucleus becomes shorter so that the nucleation is allowed also in the regime of strong connections among the cells. These two conditions, i.e., anticipated nucleation and intense "bind" among cells, determine cooperating effects, which lead to MST reduction before the saturation regime is reached.

Figures 4(b) and 4(c) show MST curves obtained in the presence of CL and LS noise sources. These behaviors appear quite different with respect to those obtained using Gaussian noise sources. MST curves are strongly affected by Lévy flights that favor jumps between different potential valleys, and soliton formation [see Fig. 5(c), containing rapid and sudden phase variations]. Specifically, for CL noise the saturation effect gives rise to a value of MST lower than that observed with the Gaussian thermal fluctuations. This is due to the peculiarity of the fat tails of the probability density function for CL noise. Therefore, for *homogeneous* density current [Fig. 4(b)], after the initial transient with an increasing behavior due to the increasing length of the junction and therefore of the string, nucleation and intense "bind" among cells speed up the escape process and τ decreases towards the saturation value. For *inhomogeneous* density current [Fig. 4(e)], the weak nonmonotonic behavior, found for the homogeneous case [see Fig. 4(b)], disappears. This is because the edge portions of the phase string are subject to high values of bias current [$i_b(x) > 1$; see Fig. 2 and Eq. (7)]. As a consequence, all the string is dragged out of the potential well, speeding up the escape process. The MST values obtained in the presence of LS noise sources are in general smaller than those obtained using noise sources with CL distribution. These differences are related to the intensity of the jumps in these two statistics. The saturation effect is also present, but the corresponding value of τ is very low. This is due to the LS Lévy flights, which push the string very quickly out of the superconductive state, giving rise to a monotonic decreasing behavior of τ versus L. In other words, LS noise drives the phase string out of the potential well very quickly, due to the greater diffusive power of this noise source. It is worth noting that, for $i_0 = 0.9$, the values obtained using the Cauchy-Lorentz statistics are slightly greater than those obtained in the presence of Gaussian thermal fluctuations. This is connected with the *limited space displacement*, which rules the CL statistics for short time scales [32].

In Figs. 4(d)–4(f), we show results obtained in the presence of an inhomogeneous bias current. According to Eq. (7), $i_b(x)$ diverges at the string ends, $x = 0$ and $x = L$, having a minimum equal to $i_b(L/2) = (2/\pi)i_0$ in the string center, $x = L/2$. In a considerable edge portion of the string (around 5% and 18% of the total length for $i_0 = 0.5$ and 0.9, respectively) $i_b(x) > 1$, allowing the phase elements to roll down along the tilted potential without encountering any resistance. We can consider these edge elements as *generators of solitons*. This corresponds to the physical situation in which the supercurrent flows between the junction ends and the fluxon formation occurs in these regions of the JJ. This kind of dynamics is shown in Fig. 5(d), in which the kink starts from the cells located in the junction edges. The role of these cells becomes particularly important as the length L increases, but it is irrelevant for short junctions, in which the connection between cells is still too strong, and the dynamics is not guided by solitons. This situation is clear in Fig. 5(b), although the presence of CL statistics causes the appearance of flights. The G curves in Fig. 4(d) show an increasing behavior similar to those obtained with homogeneous bias current distribution, even if the values reached are a little bit higher. Independently of the value of L, about 77% of the cells composing the junction have $i_b(x) < i_0$. Therefore, this percentage of cells should overcome potential barriers higher than those corresponding to the case of homogeneous bias current $i_b(x)$. This determines, in the absence of soliton formation, an increase of the escape time. Moreover, a nonmonotonic behavior is observed. After reaching the maximum, the MST curves decrease due to the action of the junction edges, which behave as generators of solitons. This effect accelerates the escape process, becoming more important as the value of L increases (see Fig. 2). For $i_0 = 0.9$, the time average of the barrier height is lower than in the case with $i_0 = 0.5$ and the switching process is faster.

The CL and LS results presented in Figs. 4(e) and 4(f) do not show remarkable differences with respect to those obtained with homogeneous current distribution, except for an enhancement in the MST for very short junction. The physical reason for this behavior is the same as that discussed for the Gaussian case.

The curves in Figs. 5(b) and 5(c), obtained using a CL noise source, show peaks associated with the generations of the Lévy flights. As previously discussed, these noise-induced fluctuations influence the switching events and the soliton formation. These graphs also clearly display the creation of another "structure" known as a *breather* [see Fig. 5(b) for $t\omega_0 = \{18.5, 19\}$ and $x/\lambda_j \approx 1.5$, and Fig. 5(c)]. This is a well-known localized solution of the SG equation consisting of a soliton-antisoliton pair and oscillating with an internal "breathing" frequency. The curves obtained by using non-Gaussian noise sources exhibit this kind of nonlinear "structure" [Figs. 5(b) and 5(c)].

B. MST versus driving frequency ω

In this section we analyze the MST behavior, setting the bias current at $i_0 = 0.9$ and varying both the frequency ω of the driving signal (within the interval [0.01,10]) and the noise intensity γ. The values of MST obtained are shown in Fig. 6. Specifically, results obtained in the presence of G, CL, and LS noise sources are shown in the top panels ([Figs. 6(a), 6(c), and 6(e)], for homogeneous bias current distribution, and in the lower panels [Figs. 6(b), 6(d), and 6(f)], for inhomogeneous bias current distribution. Each panel contains five curves, obtained for the values of γ displayed in the legend. This analysis was performed working with a junction of length $L = 10$, which is a string with a suitable length, which allows the onset of the phenomenon of soliton formation. All graphs show clearly the presence of RA [37,38,89,91–97], or *stochastic resonance activation*, a noise-induced phenomenon, whose signature is the appearance of a minimum in the curve of MST vs ω. This minimum tends to vanish for CL and LS distributions when the noise intensities are greater than the time average of the potential barrier [$\overline{\Delta U}_{i_0=0.9} \simeq 0.4$; see Eq. (22)]. It is worthwhile to note that the nonmonotonic

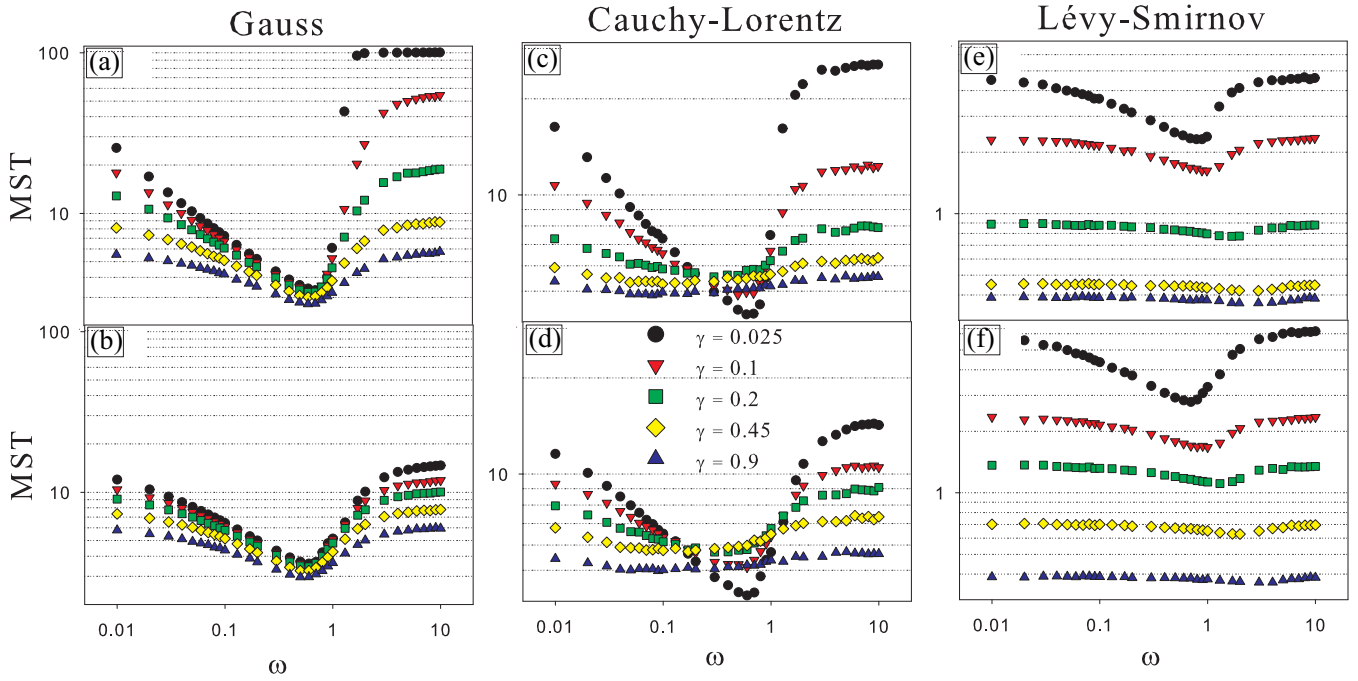

FIG. 6. (Color online) Log-log plots of MST τ vs ω obtained using homogeneous $i_b(x)$ and noise sources (a) G, (c) CL, and (e) LS, and inhomogeneous $i_b(x)$ and noise sources (b) G, (d) CL, and (f) LS. In all graphs the values of the other parameters are $i_0 = 0.9$, $L = 10$, and $\gamma = \{0.025, 0.1, 0.2, 0.45, 0.9\}$. The legend in (d) refers to all panels.

behavior of τ versus the CL noise intensity around the minimum, observed in Figs. 6(c) and 6(d), is related to that shown in Figs. 7(c) and 7(d). The RA is a phenomenon robust enough to be observed also in the presence of Lévy noise sources [32]. Particle escape from a potential well is driven when the potential barrier oscillates on a time-scale characteristic of the particle escape itself. Since the resonant frequency is close to the inverse of the average escape time at the minimum, which is the mean escape time over the potential barrier in the lower configuration, stochastic resonant activation occurs [10,43], which is a phenomenon different from the dynamic resonant activation. This effect, in fact, appears when the driving

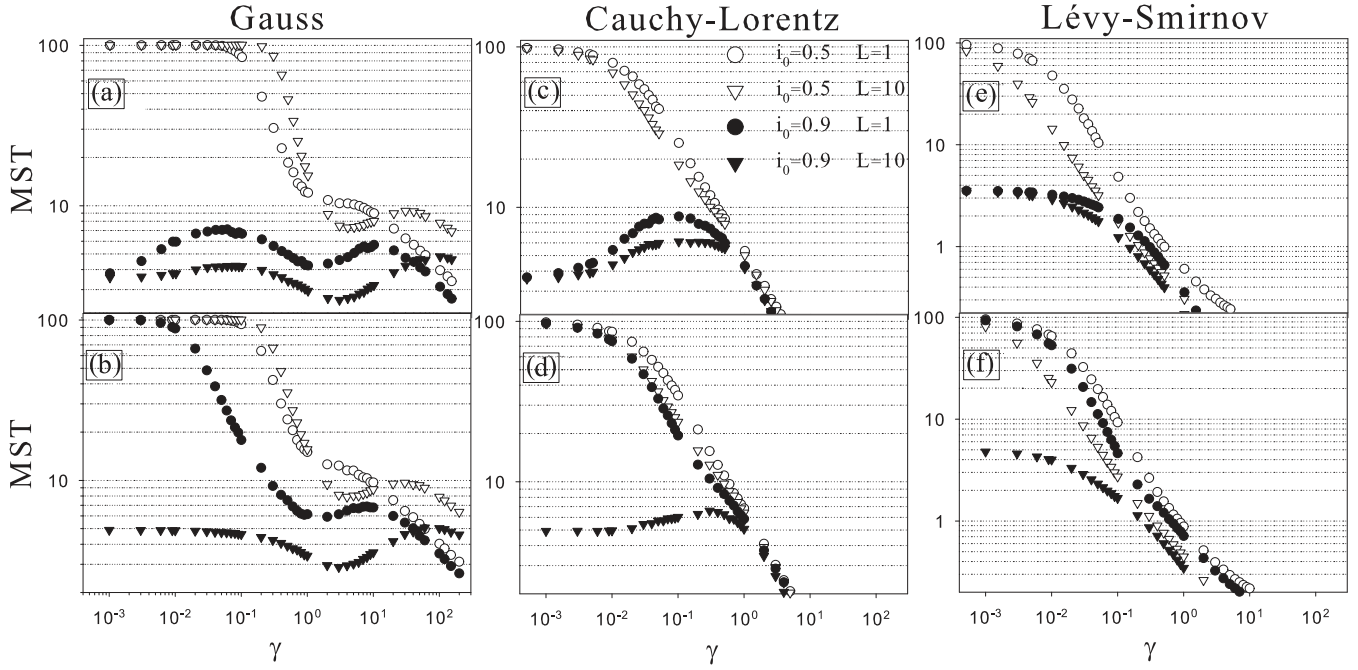

FIG. 7. Log-log plots of MST τ vs γ obtained using homogeneous $i_b(x)$ and noise sources (a) G, (c) CL, and (e) LS, and inhomogeneous $i_b(x)$ and noise sources (b) G, (d) CL, and (f) LS. In all graphs the values of other parameters are $i_0 = \{0.5, 0.9\}$, $\omega = 0.9$, and $L = \{1, 10\}$. The legend in (c) refers to all panels.

frequency matches the natural frequency of the system, that is, the plasma frequency [45,46,98]. Finally, we note that the contemporaneous presence of RA and NES phenomena in the behavior of τ as a function of the driving frequency, in underdamped JJ, has been observed, and it was found that the MST can be enhanced or lowered by using different initial conditions [42].

The G data in Figs. 6(a) and 6(b) present this minimum for a frequency value ($\omega_{RA} \sim 0.6$), which varies little with the noise intensity γ. The only evident effect, switching to an inhomogeneous bias current, is a general reduction of the MST. The curves with CL noise present a clear minimum, shifted towards higher values of ω, with respect to that of the Gaussian case. This minimum tends to disappear, increasing the noise intensity. This is due to the influence of Lévy flights which, for strong noise intensities, drive the escape processes. As found in the presence of Gaussian noise, also in the case of CL statistics, using inhomogeneous $i_b(x)$ causes a general lowering in the MST values. We can note that, for a weak noise signal, the Cauchy-Lorentz distributions are higher than the Gaussian ones: for low values of γ the jumps are not relevant, and the limited space displacement gives short phase fluctuations, making it more difficult to escape from the potential wells. The MST calculated using LS sources is also governed only by the noise and presents quite small values. Therefore, the RA effect is found only in the curve obtained for a very weak noise intensity.

By increasing the driving frequency, at low noise intensities, a trapping phenomenon occurs. A threshold frequency ω_{thr} exists such that for $\omega > \omega_{thr}$ the phase string is trapped within a region between two successive minima of the potential profile. In other words, the string cannot move from the potential well to the next valley during one period T_0 of the driving current $A\sin(\omega t)$. As a consequence, the MST diverges in the limit $\gamma \to 0$. The value of the threshold frequency increases with increasing bias current and/or maximal current across the junction [28,40,89]. We have estimated the threshold values for the following parameter values: $i_0 = 0.9$ and $A = 0.7$. Specifically, for Gaussian thermal fluctuations $\omega_{thr} \gtrsim 1.8$, for the CL noise source $\omega_{thr} \gtrsim 2.1$, and for the LS noise source $\omega_{thr} \gtrsim 3$.

C. MST versus noise intensity γ

Here we analyze the MST curves calculated by varying the noise amplitude in the range [0.0005,200]. The results are shown in Fig. 7. Specifically the results in Figs. 7(a), 7(c), and 7(e) were obtained using a homogeneous $i_b(x)$ and G, CL, and LS noise sources, respectively, while those shown in Figs. 7(b), 7(d), and 7(f) were obtained using an inhomogeneous $i_b(x)$ and G, CL, and LS noise sources, respectively. This analysis is performed using $\omega = 0.9$ and two different values of L and i_0, i.e., $L = \{1,10\}$ and $i_0 = \{0.5,0.9\}$. Fixing the values of the system parameters, for $\gamma \to 0$ the curves for the three noise sources (G, CL, and LS) converge to the same values, i.e., the deterministic lifetime in the superconducting state, which depend strongly on the bias current. When $\gamma \to 0$ and the potential is not too tilted, trapping phenomena occur, and the MST tends to t_{max}. Increasing the noise intensity, the MST curves exhibit an effect of NES [39,40,89,99–110], a noise-induced phenomenon consisting of a nonmonotonic behavior with the appearance of a maximum. The stability of metastable states can be enhanced and the average lifetime of the metastable state increases nonmonotonically with the noise intensity. The observed nonmonotonic resonancelike behavior proves to be different from the monotonic one of the Kramers theory and its extensions [111–113]. This enhancement of stability, first noted by Hirsch *et al.* [114], has been observed in different physical and biological systems and belongs to a highly topical interdisciplinary research field, ranging from condensed matter physics to molecular biology to cancer growth dynamics [103,115].

From Fig. 7, we note that in the curve obtained using a Gaussian noise source, homogeneous current distribution, and high washboard inclination, $i_0 = 0.9$, two maxima are present in correspondence of $\gamma_{max}^{L=1} \cong \{0.06,10\}$ for $L = 1$ and $\gamma_{max}^{L=10} \cong \{0.07,100\}$ for $L = 10$. In view of understanding the physical motivations of these NES effects, we calculate the time evolution of the probability $P(t)$, as defined in Eq. (20), during the switching dynamics of the junction. We remember that $0 \leqslant P(t) \leqslant 1$, where the two extreme values indicate the resistive state $[P(t) = 0]$ and the superconducting state $[P(t) = 1]$.

The time evolution of $P(t)$ was calculated for $i_0 = 0.9$ and $\omega = 0.9$. The results, shown in Fig. 8, were obtained in the following conditions: (i) G noise with $L = 1$ [Fig. 8(a)] and $L = 10$ [Fig. 8(b)]; (ii) CL noise with $L = 10$ [Fig. 8(c)]. All panels of Fig. 8 contain curves of $P(t)$ calculated by setting the noise intensity at values for which a maximum or minimum appears in the MST vs γ behavior (see insets). Looking at the curves displayed in Fig. 8(a), we note that the dotted curve ($\gamma = 0.0005$) represents a deterministic switching event. The string after a quick escape does not return inside the first washboard valley. Conversely, the dashed line, obtained for $\gamma = 0.06$, describes a temporary trapping phenomenon. The contemporaneous presence of the fluctuating potential and noise source inhibits the phase switching and therefore the passage of the junction to the resistive regime. Moreover, the exit from the first well is not sharp, as in the deterministic case, and $P(t)$ assumes an oscillatory behavior, almost in resonance with the periodical motion of the washboard potential. This oscillating behavior of $P(t)$, which is related to the temporary trapping of the phase string, tends to disappear as the noise intensity increases. For $\gamma = 10$ [solid line in Fig. 8(a)], another peak (NES effect) in the MST behavior is observed, but no oscillations in $P(t)$ are present. At this value of γ, the JJ dynamics is totally driven by the noise and the NES effect is due to the possibility that the phase string returns into the first valley after a first escape event, as indicated by the fat tail of $P(t)$. This behavior is strictly connected to that found for the MST, whose calculation is based on the definition of NLRT. Further increases of γ reduce for the phase string the possibility not only of returning into the initial well but also of staying for a long time inside it. The results for G noise source and $L = 10$, displayed in Fig. 8(b), are similar to those obtained for $L = 1$. The first hump, corresponding to $\gamma = 0.07$ [see inset of Fig. 8(b)] is a little bit smaller than that for $L = 1$ and $\gamma = 0.06$ [see inset of Fig. 8(a)], and this is consistent with the previous MST vs L analysis. Moreover, a NES effect

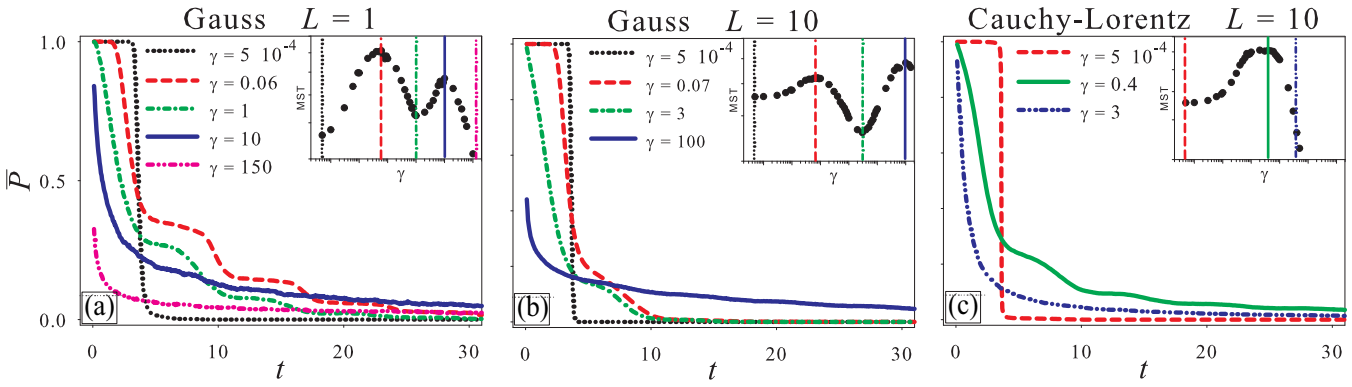

FIG. 8. (Color online) Time evolution of the probability $P(t)$ in the following conditions: G noise with (a) $L = 1$ and (b) $L = 10$; (c) CL noise with $L = 10$. The system parameters are $i_0 = 0.9$ and $\omega = 0.9$. Each graph contains curves of $P(t)$ obtained using values of γ for which a minimum or maximum appears in the τ vs γ behavior. The insets reproduce the corresponding curves of Figs. 7(a) and 7(c).

for $\gamma = 100$ is present [see inset of Fig. 8(b)]. We note the difference of one order of magnitude in the noise intensity ($\gamma = 100$ for $L = 10$) with respect to the NES phenomenon observed for $L = 1$ at $\gamma = 10$. This difference is due to the greater difficulty for random fluctuations of carrying a string, ten times longer, again in the initial potential well. Figure 7(c) shows the curves of MST vs γ in the presence of a CL noise source. Here we note the absence of the second peak, observed in the previous analysis at higher values of γ. This discrepancy can be explained by noting that, for low noise intensity, the effect of the CL flights on the overall JJ dynamics is negligible, and the time evolution should appear quite similar to those observed with Gaussian noise. Conversely, due to the limited space displacement, to obtain the same effect (i.e., escape from the first potential well), junctions subject to CL noise should be exposed to noise intensity larger with respect to identical junctions subject to G noise. The peak (maximum of MST) should be therefore shifted towards higher values of γ. Increasing the noise intensity, the influence of Lévy flights on the total JJ dynamics becomes higher, and the probability that a second peak appears, similar to that observed in the presence of G noise, tends to vanish. This analysis is confirmed by the graph shown in Fig. 8(c). Conversely, LS flights are too intense to allow the formation of NES peaks [see Fig. 7(e)]. Finally, we note that the curves obtained with inhomogeneous $i_b(x)$ do not present any differences, except those for $i_0 = 0.9$ and $L = 1$ (solid circles), which show very high values of MST with respect to the case of homogenous current distribution. This indicates again a trapping phenomenon that occurs when a short junction undergoes very weak noise intensities ($\gamma \to 0$). In this case, the parts of the junction generating solitons do not affect the string dynamics. In fact, since $i_b(x) < i_0$ for 77% of the total length, a large percentage of the string remains confined in a potential well deeper than that of the analogous homogeneous case, thus determining the trapping effect.

Moreover, all the curves of MST vs γ for CL and LS noise sources coalesce together at high noise intensities. The MST has a power-law dependence on the noise intensity according to the expression

$$\tau \simeq \frac{C(\alpha)}{\gamma^{\mu(\alpha)}}, \tag{23}$$

where the prefactor C and the exponent μ depend on the Lévy index α [55]. From Fig. 7 we have $\mu(\alpha) \sim 0.9$ for CL noise and $\mu(\alpha) \sim 1.2$ for LS noise, which are in agreement with the exponent $\mu(\alpha) \approx 1$ for $0 < \alpha < 2$, calculated for barrier crossing in bistable and metastable potential profiles [116,117].

VI. SIMULTANEOUS PRESENCE OF LÉVY NOISE AND THERMAL FLUCTUATIONS

In this section we analyze the presence of both thermal and Lévy noise sources. Therefore, in Eqs. (1) and (2) both contributions of Gaussian thermal fluctuating current density $i_T(x,t)$ and non-Gaussian Lévy noise current density $i_{nG}(x,t)$ are considered. The Lévy contribution is restricted to a Cauchy-Lorentz term. The noise intensities are indicated by γ_G (Gaussian), ranging within the interval $[10^{-7},1]$, and γ_{CL} (Cauchy-Lorentz). Noise-induced phenomena previously observed when the CL noise source only is present show now some differences. The values of the system parameters are chosen in such a way to highlight these changes. Figure 9 contains a collection of MST curves obtained by varying the junction length L [Figs. 9(a) and 9(b)], CL noise intensity γ_{CL} [Figs. 9(c) and 9(d)], and frequency of the oscillating bias current ω [Figs. 9(e) and 9(f)]. Top and bottom panels show data calculated using $i_0 = 0.5$ and $i_0 = 0.9$, respectively. An overall reduction of the MST values is observed by increasing the intensity of thermal fluctuations, by speeding up the switching process between the superconductive and the resistive state. The simultaneous presence of thermal fluctuations and a Lévy noise source produces an increase of the overall intensity "felt" by the string phase. In all panels clear modifications of the nonmonotonic behavior are present, becoming more pronounced as the Gaussian thermal noise intensity increases, especially for $\gamma_G > 10^{-1}$.

The analysis of MST vs L suggests that the soliton dynamics is modified only when the intensities of the thermal fluctuations are greater than those of the CL noise, that is, $\gamma_G > \gamma_{CL}$; conversely the curves for $\gamma_G < \gamma_{CL}$ overlap altogether ($\gamma_G \leqslant 10^{-1}$). The curves of Figs. 9(a) and 9(b) maintain the structure already shown in Fig. 4(b) (see Sec. V A), which is a nonmonotonic behavior with a maximum and a saturation plateau. The saturation value of τ decreases, of course, with the increase of the intensity of thermal fluctuations.

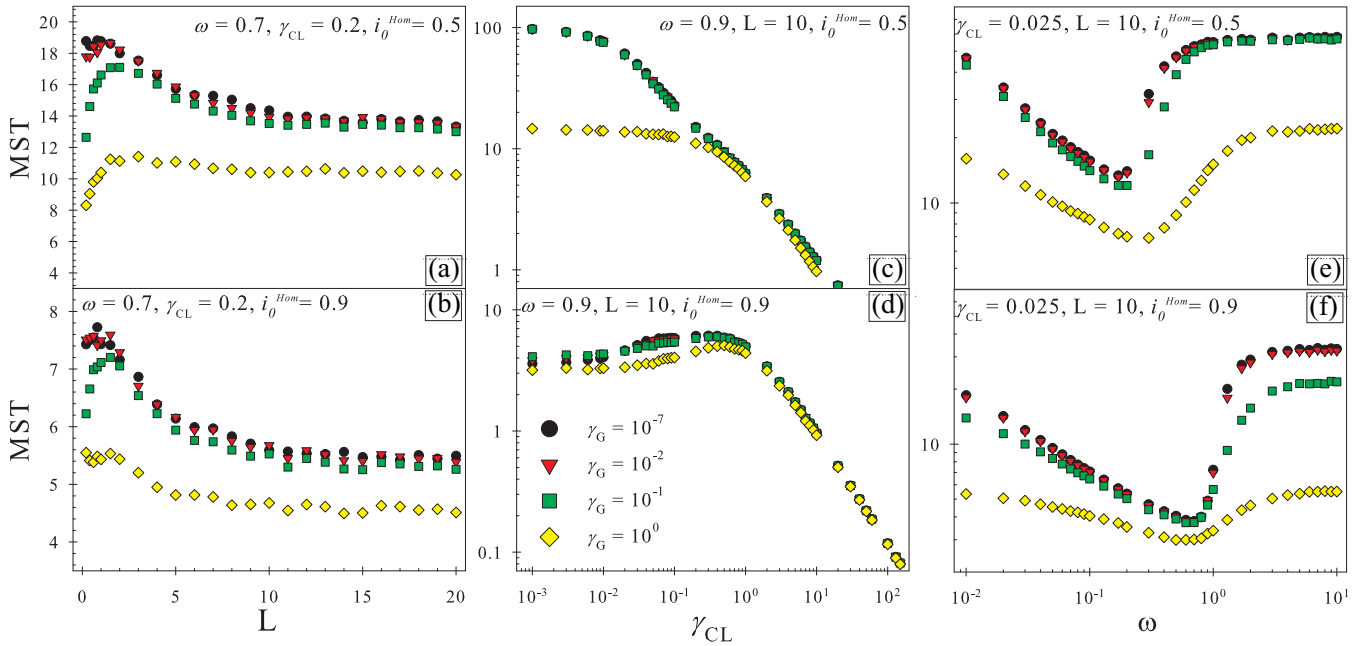

FIG. 9. (Color online) MST τ as a function of L, $\gamma_{\rm CL}$, and ω. All curves were obtained considering the simultaneous presence of CL and thermal noise sources, using two different values, i.e., (a, c, e) $i_0 = 0.5$ and (b, d, f) $i_0 = 0.9$, of the homogenous bias current, and varying the Gaussian noise intensity, $\gamma_{\rm G}$. The legend in (d) refers to all panels.

Looking at the graphs of MST vs $\gamma_{\rm CL}$ [Fig. 9(c)], trapping phenomena are observed when $\gamma_{\rm CL} \to 0$ and $\gamma_{\rm G} \to 0$. For $\gamma_{\rm G} \geqslant 1$, that is, when the Gaussian thermal noise intensity is comparable with the time average of the potential barrier height [$\overline{\Delta U}_{i_0=0.5} \simeq 1$; see Eq. (22)], trapping events disappear and thermally activated processes drive the switching events. For $i_0 = 0.9$ [Fig. 9(d)] all the curves show a nonmonotonic behavior, which is the signature of the NES effect. Low thermal noise intensities do not affect the behavior of the NES curve, with respect to the case of absence of thermal noise, until their value is lower than $\gamma_G \simeq 0.2$. This is the value of the CL noise intensity corresponding to the maximum of τ vs $\gamma_{\rm CL}$, $\gamma_{\rm CL}^{\rm max} \simeq 0.2$ [see Fig. 7(c)]. In other words, thermal fluctuations affect the behavior of the NES curve for $\gamma_{\rm G} \gtrsim \gamma_{\rm CL}^{\rm max}$. The maximum of the curve decreases and it is shifted towards higher CL noise intensities because of the larger spatial region of the potential profile spanned by the phase string before reaching the boundaries $[-\pi,\pi]$.

For CL noise intensities $\gamma_{\rm CL} \gtrsim 1$, all the curves of MST vs $\gamma_{\rm CL}$ [see Figs. 9(c) and 9(d)] coalesce together with a power-law behavior given by Eq. (23), with $\mu(\alpha) \sim 0.9$. When the structure of the potential profile becomes irrelevant for the dynamics of the phase string, that is, when the noise intensity $\gamma_{\rm CL}$ is greater than the time average of the potential barrier heights ($\overline{\Delta U}_{i_0=0.5} \simeq 1$ and $\overline{\Delta U}_{i_0=0.9} \simeq 0.4$), the MST has a power-law dependence on the noise intensity.

The curves of MST as a function of ω in Figs. 9(e) and 9(f) reproduce the typical RA behavior [see Figs. 6(c) and 6(d)]. Again, all the curves of MST are lowered for increasing thermal fluctuation intensities. Specifically, for $i_0 = 0.5$ [Fig. 9(e)], the minimum of the curve decreases and it is shifted towards higher values of the driving frequency. The resonant rate escape, that is, the resonant frequency at the minimum, increases by increasing the overall noise intensity, where the height of the average potential barrier is fixed ($\overline{\Delta U}_{i_0=0.5} \simeq 1$). For $i_0 = 0.9$ [Fig. 9(f)], there is not any potential barrier for about half a period of the external driving force, and therefore the switching process is accelerated, and the position of the minimum is slightly affected by thermal fluctuations.

VII. CONCLUSIONS

We have investigated the influence of both thermal fluctuations and external non-Gaussian noise sources on the temporal characteristics of long-overlap JJs. We studied how random fluctuations with different α-stable (or Lévy) distributions affect the superconducting lifetime of long current-biased Josephson junctions. The study was performed within the framework of the sine-Gordon equation. Specifically we analyzed the MST of the phase difference across the junction, from a minimum of the tilted washboard potential, as a function of different parameters of the system and external random and periodical driving signals. We found nonmonotonic behaviors of the superconducting lifetime τ as a function of noise intensity γ, driving frequency ω, and junction length L.

In particular, in the behavior of the MST, we observed noise-induced phenomena such as stochastic resonant activation and noise-enhanced stability, with different characteristics depending on both the bias current distribution along the junction and the length of the superconducting device. Moreover, temporary trapping of the phase string in the metastable state with Gaussian thermal and CL noises gives rise to an oscillating behavior of the time evolution of the probability $P(t)$. The analysis of the MST as a function of the junction length revealed that the soliton dynamics plays a crucial role in the switching dynamics from the superconducting to the resistive

state. In more detail, we studied the relationship between creation and propagation of solitons and different features of the mean switching time. This analysis has demonstrated the existence of two different dynamical regimes. One, occurring for short junctions, is characterized by the movement of the phase string as a whole. The other one occurs for junctions whose size exceeds a critical length, in which the kink (or antikink) creation is allowed.

Moreover, for high values of the bias current, there is a length in which the two regimes take place simultaneously. Finally we found that, choosing an inhomogeneous distribution of the bias current along the junction, the cells located at the junction edges behave as generators of solitons. In these conditions the escape from the metastable superconducting state is strongly affected by the soliton dynamics. The analysis of the contemporaneous presence of Cauchy-Lorentz and thermal noise sources gives rise to modifications in the soliton dynamics and noise-induced effects observed in the transient dynamics of JJs in the presence of non-Gaussian, Lévy-type noise sources. Moreover, oscillating pairs of soliton-antisoliton (breathers) induced by the noise have been observed.

Our findings, which are important to understand the physics of fluctuations in long-overlap Josephson junctions to improve the performance of these devices, could help to shed new light on the general context of the nonequilibrium statistical mechanics. In fact, JJs are good candidates for probing relevant physics issues in metastable systems [42]. Moreover, the mean switching time from one of the metastable states of the potential profile encodes information on the non-Gaussian background noise. Therefore, the statistical analysis of the switching times of JJs can be used to analyze weak signals in the presence of an unknown non-Gaussian background noise.

ACKNOWLEDGMENT

The authors acknowledge the financial support of the Ministry of Education, University, and Research of the Italian Government (MIUR).

[1] G. Wendin and V. S. Shumeiko, Low Temp. Phys. **33**, 724 (2007).
[2] Ju H. Kim, R. P. Dhungana, and K. S. Park, Phys. Rev. B **73**, 214506 (2006).
[3] A. B. Zorin, E. M. Tolkacheva, M. I. Khabipov, F. I. Buchholz, and J. Niemeyer, Phys. Rev. B **74**, 014508 (2006).
[4] A. J. Berkley, H. Xu, M. A. Gubrud, R. C. Ramos, J. R. Anderson, C. J. Lobb, and F. C. Wellstood, Phys. Rev. B **68**, 060502 (2003).
[5] C. H. Wu, Y. T. Chou, W. C. Kuo, J. H. Chen, L. M. Wang, J. C. Chen, U. C. Sou, H. C. Yang, and J. T. Jeng, Nanotechnology **19**, 315304 (2008).
[6] E. M. Levenson-Falk, R. Vijay, N. Antler, and I. Siddiqi, Supercond. Sci. Technol. **26**, 055015 (2013).
[7] H. Grabert, Phys. Rev. B **77**, 205315 (2008).
[8] D. F. Urban and H. Grabert, Phys. Rev. B **79**, 113102 (2009).
[9] G. Filatrella and V. Pierro, Phys. Rev. E **82**, 046712 (2010).
[10] P. Addesso, G. Filatrella, and V. Pierro, Phys. Rev. E **85**, 016708 (2012).
[11] P. Reimann, C. Van den Broeck, H. Linke, P. Hänggi, J. M. Rubi, and A. Pérez-Madrid, Phys. Rev. Lett. **87**, 010602 (2001).
[12] A. A. Dubkov and B. Spagnolo, Phys. Rev. E **72**, 041104 (2005).
[13] H. Xu, A. J. Berkley, R. C. Ramos, M. A. Gubrud, P. R. Johnson, F. W. Strauch, A. J. Dragt, J. R. Anderson, C. J. Lobb, and F. C. Wellstood, Phys. Rev. B **71**, 064512 (2005).
[14] B. Huard, H. Pothier, N. O. Birge, D. Esteve, X. Waintal, and J. Ankerhold, Ann. Phys. **16**, 736 (2007).
[15] T. Novotný, J. Stat. Mech.: Theory Exp. (2009) P01050.
[16] Q. Le Masne, H. Pothier, N. O. Birge, C. Urbina, and D. Esteve, Phys. Rev. Lett. **102**, 067002 (2009).
[17] L. Billings, M. I. Dykman, and I. B. Schwartz, Phys. Rev. E **78**, 051122 (2008).
[18] J. T. Peltonen, A. V. Timofeev, M. Meschke, T. T. Heikkilä, and J. P. Pekola, Physica E **40**, 111 (2007).
[19] J. Tobiska and Yu. V. Nazarov, Phys. Rev. Lett. **93**, 106801 (2004).
[20] E. W. Montroll and M. F. Shlesinger, *Nonequilibrium Phenomena II: From Stochastics to Hydrodynamics*, edited by J. L. Lebowitz and E. W. Montroll (North-Holland, Amsterdam, 1984).
[21] M. F. Shlesinger, G. M. Zaslavsky, and U. Frisch, *Lévy Flights and Related Topics in Physics* (Springer-Verlag, Berlin, 1995).
[22] B. Dybiec and E. Gudowska-Nowak, Phys. Rev. E **69**, 016105 (2004).
[23] M. R. Souryal, E. G. Larsson, B. Peric, and B. R. Vojcic, IEEE Trans. Signal Process. **56**, 266 (2008).
[24] J. Ankerhold, Phys. Rev. Lett. **98**, 036601 (2007).
[25] E. V. Sukhorukov and A. N. Jordan, Phys. Rev. Lett. **98**, 136803 (2007).
[26] M. Köpke and J. Ankerhold, New J. Phys. **15**, 043013 (2013).
[27] A. V. Gordeeva and A. L. Pankratov, Appl. Phys. Lett. **88**, 022505 (2006).
[28] A. V. Gordeeva and A. L. Pankratov, J. Appl. Phys. **103**, 103913 (2008).
[29] A. L. Pankratov and B. Spagnolo, Phys. Rev. Lett. **93**, 177001 (2004).
[30] G. Augello, D. Valenti, and B. Spagnolo, Int. J. Quantum Inf. **06**, 801 (2008).
[31] A. V. Gordeeva, A. L. Pankratov, and B. Spagnolo, Int. J. Bifurcation Chaos Appl. Sci. Eng. **18**, 2825 (2008).
[32] G. Augello, D. Valenti, and B. Spagnolo, Eur. Phys. J. B **78**, 225 (2010).
[33] G. Augello, D. Valenti, A. L. Pankratov, and B. Spagnolo, Eur. Phys. J. B **70**, 145 (2009).
[34] K. G. Fedorov and A. L. PankratovPhys. Rev. B **76**, 024504 (2007).
[35] K. G. Fedorov, A. L. Pankratov, and B. Spagnolo, Int. J. Bifurcation Chaos Appl. Sci. Eng. **18**, 2857 (2008).
[36] K. G. Fedorov and A. L. Pankratov, Phys. Rev. Lett. **103**, 260601 (2009).
[37] C. R. Doering and J. C. Gadoua, Phys. Rev. Lett. **69**, 2318 (1992).

[38] R. N. Mantegna and B. Spagnolo, Phys. Rev. Lett. **84**, 3025 (2000).

[39] R. N. Mantegna and B. Spagnolo, Phys. Rev. Lett. **76**, 563 (1996).

[40] N. V. Agudov and B. Spagnolo, Phys. Rev. E **64**, 035102(R) (2001).

[41] Y. Yu and S. Han, Phys. Rev. Lett. **91**, 127003 (2003).

[42] G. Sun, N. Dong, G. Mao, J. Chen, W. Xu, Z. Ji, L. Kang, P. Wu, Y. Yu, and D. Xing, Phys. Rev. E **75**, 021107 (2007).

[43] C. Pan, X. Tan, Y. Yu, G. Sun, L. Kang, W. Xu, J. Chen, and P. Wu, Phys. Rev. E **79**, 030104(R) (2009).

[44] P. Febvre, D. Bouis, N. De Leo, M. Fretto, A. Sosso, and V. Lacquaniti, J. Appl. Phys. **107**, 103927 (2010).

[45] M. H. Devoret, J. M. Martinis, D. Esteve, and J. Clarke, Phys. Rev. Lett. **53**, 1260 (1984).

[46] M. H. Devoret, J. M. Martinis, and J. Clarke, Phys. Rev. Lett. **55**, 1908 (1985).

[47] M. G. Castellano, G. Torrioli, C. Cosmelli, A. Costantini, F. Chiarello, P. Carelli, G. Rotoli, M. Cirillo, and R. L. Kautz, Phys. Rev. B **54**, 15417 (1996).

[48] S. Han, Y. Yu, X. Chu, S.-I. Chu, and Z. Wang, Science **293**, 1457 (2001).

[49] Y. Yu, Y. Zhang, W. Qiu, S. Li, S. Han, and Z. Wang, Supercond. Sci. Technol. **15**, 555 (2002).

[50] W. Szajnowski and J. Wynne, IEEE Signal Process. Lett. **8**, 151 (2001).

[51] A. V. Chechkin, V. Yu. Gonchar, J. Klafter, and R. Metzler, Adv. Chem. Phys. Part B **133**, 439 (2006).

[52] R. Metzler and J. Klafter, Phys. Rep. **339**, 1 (2000).

[53] V. V. Uchaikin, Phys.-Usp. **46**, 821 (2003).

[54] A. A. Dubkov, A. La Cognata, and B. Spagnolo, J. Stat. Mech.: Theory Exp. (2009) P01002.

[55] A. A. Dubkov, B. Spagnolo, and V. V. Uchaikin, Int. J. Bifurcation Chaos Appl. Sci. Eng. **18**, 2649 (2008).

[56] B. J. West and W. Deering, Phys. Rep. **246**, 1 (1994).

[57] A. M. Reynolds, J. Phys. A: Math. Theor. **42**, 434006 (2009).

[58] D. W. Sims *et al.*, Nature (London) **451**, 1098 (2008).

[59] A. M. Reynolds, Ecology **89**, 2347 (2008).

[60] D. Brockmann, L. Hufnagel, and T. Geisel, Nature (London) **439**, 462 (2006).

[61] R. N. Mantegna and H. E. Stanley, Nature (London) **376**, 46 (1995).

[62] M. F. Shlesinger, *Lecture Notes in Physics Vol. 450* (Springer-Verlag, Berlin, 1971).

[63] P. D. Ditlevsen, Geophys. Res. Lett. **26**, 1441 (1999).

[64] A. Barone and G. Paternò, *Physics and Applications of the Josephson Effect* (Wiley, New York, 1982).

[65] K. K. Likharev, *Dynamics of Josephson Junctions and Circuits* (Gordon and Breach, New York, 1986).

[66] A. V. Ustinov, Physica D **123**, 315 (1998).

[67] M. Büttiker and R. Landauer, Phys. Rev. A **23**, 1397 (1981).

[68] D. W. McLaughlin and A. C. Scott, Phys. Rev. A **18**, 1652 (1978).

[69] B. Dueholm, E. Joergensen, O. Levring, R. Monaco, J. Mygind, N. Pedersen, and M. Samuelsen, IEEE Trans. Magn. **19**, 1196 (1983).

[70] A. A. Abdumalikov, M. V. Fistul, and A. V. Ustinov, Phys. Rev. B **72**, 144526 (2005).

[71] J. Pfeiffer, M. Schuster, A. A. Abdumalikov, Jr., and A. V. Ustinov, Phys. Rev. Lett. **96**, 034103 (2006).

[72] K. G. Fedorov, M. V. Fistul, and A. V. Ustinov, Phys. Rev. B **84**, 014526 (2011).

[73] J. H. Kim, B. R. Ghimire, and H. Y. Tsai, Phys. Rev. B **85**, 134511 (2012).

[74] A. L. Pankratov, A. V. Gordeeva, and L. S. Kuzmin, Phys. Rev. Lett. **109**, 087003 (2012).

[75] M. A. García-Ñustes and J. A. González, Phys. Rev. E **86**, 066602 (2012).

[76] D. R. Gulevich, M. B. Gaifullin, and F. V. Kusmartsev, Eur. Phys. J. B **85**, 24 (2012).

[77] G. C. Wick, Rev. Mod. Phys. **27**, 339 (1955).

[78] M. R. Samuelsen and S. A. Vasenko, J. Appl. Phys. **57**, 110 (1985).

[79] W. A. Woyczynski, in *Lévy Processes: Theory and Applications*, edited by O. E. Barndorff-Nielsen, T. Mikosch, and S. I. Resnick (Birkhäuser, Boston, 2001), p. 241.

[80] J. Bertoin, *Lévy Processes* (Cambridge University Press, Cambridge, 1996).

[81] K. I. Sato, *Lévy Processes and Infinitely Divisible Distributions* (Cambridge University Press, Cambridge, 1999).

[82] B. V. Gnedenko and A. N. Kolmogorov, *Limit Distributions for Sums of Independent Random Variables* (Addison-Wesley, Cambridge, MA, 1954).

[83] B. de Finetti, *Theory of Probability* (Wiley, New York, 1975), Vols. 1 and 2.

[84] A. Khintchine and P. Lévy, C. R. Acad. Sci. Paris **202**, 374 (1936).

[85] A. Ya. Khintchine, *Limit Distributions for the Sum of Independent Random Variables* (ONTI, Moscow, 1938).

[86] W. Feller, *An Introduction to Probability Theory and Its Applications* (John Wiley & Sons, New York, 1971), Vol. 2.

[87] A. Weron, Stat. Probab. Lett. **28**, 165 (1996).

[88] J. M. Chambers, C. L. Mallows, and B. W. Stuck, J. Am. Stat. Assoc. **71**, 340 (1976).

[89] A. A. Dubkov, N. V. Agudov, and B. Spagnolo, Phys. Rev. E **69**, 061103 (2004).

[90] A. N. Malakhov and A. L. Pankratov, Adv. Chem. Phys. **121**, 357 (2002).

[91] R. N. Mantegna and B. Spagnolo, J. Phys. IV (France) **08**, Pr6-247 (1998).

[92] P. Pechukas and P. Hänggi, Phys. Rev. Lett. **73**, 2772 (1994).

[93] M. Marchi, F. Marchesoni, L. Gammaitoni, E. Menichella-Saetta, and S. Santucci, Phys. Rev. E **54**, 3479 (1996).

[94] B. Dybiec and E. Gudowska-Nowak, J. Stat. Mech.: Theory Exp. (2009) P05004.

[95] S. Miyamoto, K. Nishiguchi, Y. Ono, K. M. Itoh, and A. Fujiwara, Phys. Rev. B **82**, 033303 (2010).

[96] Y. Hasegawa and M. Arita, Phys. Lett. A **375**, 3450 (2011).

[97] A. Fiasconaro and B. Spagnolo, Phys. Rev. E **83**, 041122 (2011).

[98] J. M. Martinis, M. H. Devoret, and J. Clarke, Phys. Rev. B **35**, 4682 (1987).

[99] B. Spagnolo, N. V. Agudov, and A. A. Dubkov, Acta Phys. Pol. B **35**, 1419 (2004).

[100] P. D'Odorico, F. Laio, and L. Ridolfi, Proc. Natl. Acad. Sci. USA **102**, 10819 (2005).

[101] A. Fiasconaro, B. Spagnolo, and S. Boccaletti, Phys. Rev. E **72**, 061110 (2005).

[102] P. I. Hurtado, J. Marro, and P. L. Garrido, Phys. Rev. E **74**, 050101 (2006).
[103] B. Spagnolo, A. A. Dubkov, A. L. Pankratov, E. V. Pankratova, A. Fiasconaro, and A. Ochab-Marcinek, Acta Phys. Pol. B **38**, 1925 (2007).
[104] R. Mankin, E. Soika, A. Sauga, and A. Ainsaar, Phys. Rev. E **77**, 051113 (2008).
[105] M. Yoshimoto, H. Shirahama, and S. Kurosawa, J. Chem. Phys. **129**, 014508 (2008).
[106] A. Fiasconaro and B. Spagnolo, Phys. Rev. E **80**, 041110 (2009).
[107] M. Trapanese, J. Appl. Phys. **105**, 07D313 (2009).
[108] A. Fiasconaro, J. J. Mazo, and B. Spagnolo, Phys. Rev. E **82**, 041120 (2010).
[109] J.-H. Li and J. Łuczka, Phys. Rev. E **82**, 041104 (2010).
[110] A. A. Smirnov and A. L. Pankratov, Phys. Rev. B **82**, 132405 (2010).
[111] H. A. Kramers, Physica **7**, 284 (1940).
[112] V. I. Melnikov, Phys. Rep. **209**, 1 (1991).
[113] P. Hänggi, P. Talkner, and M. Borkovec, Rev. Mod. Phys. **62**, 251 (1990).
[114] J. E. Hirsch, B. A. Huberman, and D. J. Scalapino, Phys. Rev. A **25**, 519 (1982).
[115] B. Spagnolo, P. Caldara, A. La Cognata, G. Augello, D. Valenti, A. Fiasconaro, A. A. Dubkov, and G. Falci, Acta Phys. Pol. B **43**, 1169 (2012).
[116] A. V. Chechkin, V. Y. Gonchar, J. Klafter, and R. Metzler, Europhys. Lett. **72**, 348 (2005).
[117] A. V. Chechkin, O. Y. Sliusarenko, R. Metzler, and J. Klafter, Phys. Rev. E **75**, 041101 (2007).